

A High Temperature Lithium-Aluminum Alloy/Oxygen or Air Fuel Cell

Sarwan S. Sandhu

Department of Chemical and Materials Engineering, University of Dayton 300 College Park, Dayton, OH 45469, USA

ARTICLE INFO

Published Online:
07 January 2025

ABSTRACT

The work reported in this paper is in support of our current effort in the development of an experimental hybrid (lithium-aluminum alloy/electrolyte/oxygen or air) fuel cell for the acquisition of the experimental data required to characterize its performance behavior.

The literature-based assembled formulation provided in this paper can be used to predict the cell open-circuit electric potential, lithium amount in the cell anode alloy, and g-atom ratio of lithium to aluminum in the cell anode as a function of time at any cell discharge current level. The ohmic voltage losses can also be computed in the cell cathode, anode, and two electrolytes at a cell current level.

The computed ohmic-voltage loss data in the various components of the cell (Figure 1 in Section 1), during its discharge; for example, at the geometric current density of $0.10 \text{ amp} \cdot \text{cm}_{geom}^{-2}$ at the cell temperature of $405 \text{ }^\circ\text{C}$ is presented in the paper. The computed data are summarized as given below:

1. The predicted open-circuit cell voltage at $405 \text{ }^\circ\text{C}$ is 2.3241 volt .
2. At the geometric current density of $0.10 \text{ amp} \cdot \text{cm}_{geom}^{-2}$, the ohmic voltage loss in the cell anode is relatively negligible. The ohmic voltage loss in the electrolyte-1, electrolyte-2, and cathode is 1.3620 , 0.0048 , and 0.0002 volt , respectively. The ohmic cell voltage loss in the electrolyte-1 of thickness $10 \mu\text{m}$ is dominant. It is, therefore, suggested that the electrolyte-1 membrane thickness be less than $5 \mu\text{m}$ to reduce the overall cell operational voltage loss at any discharge current level.
3. The predicted operational cell voltage, at the cell discharge current of $0.10 \text{ amp} \cdot \text{cm}_{geom}^{-2}$ is about 0.9571 volt at the cell temperature of $405 \text{ }^\circ\text{C}$.

Corresponding Author:
Sarwan S. Sandhu

1. INTRODUCTION

To improve the efficiency of a lithium-oxygen or air fuel cell, our very recent engagement has been in the design and

development of an experimental cell of the type sketched in Figure 1:

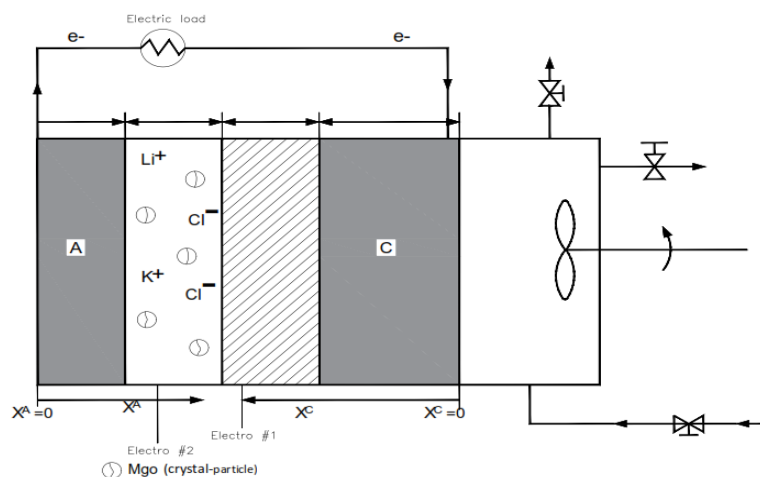


Figure 1: High-temperature Lithium – oxygen or air fuel cell (the above sketch not to a scale)

It consists of a cathode (C): Porous strontia-doped lanthanum manganite perovskite, $\text{La}_{1-x}\text{Sr}_x\text{MnO}_3$; $0.1 < x < 0.15$. The cell cathode-side reactant is pure dry oxygen or air. The oxidant oxygen or air is caused to flow through a cathode-side chamber. The oxidant is stirred to acquire high fluid-flow turbulence levels to achieve the uniform molar concentration of oxygen at the surface, located at $X^C = 0$ plane, of the porous solid cathode electrode as well as to reduce the thickness of the species concentration boundary-layer likely to exist there; thus, reducing the resistance to mass transfer of oxygen or enhancing the oxygen molar flux to the porous cathode surface located at $X^C = 0$ plane.

Electrolyte #1 (Electro #1): It is the solid solution of scandia – in – zirconia, $(\text{ZrO}_2)_{1-x}(\text{Sc}_2\text{O}_3)_x$; with $x = 0.06, 0.09, 0.10$ or 0.11 of $\text{Sc}_2\text{O}_3(s)$ in the mixture with zirconia as the solid-state solvent (for the oxide ion, O^{2-} , transport); with the negligible electronic transport between the cell cathode and the electrolyte #2.

Electrolyte #2 (Electro #2): It is the eutectic mixture of lithium chloride (LiCl) and potassium chloride (KCl); with magnesium oxide ($\text{MgO}(s)$) solid ceramic particles as the immiscible agent for the eutectic mixture of lithium chloride and potassium chloride.

Cell anode (A): It is a lithium–aluminum alloy in contact with the electrolyte #2.

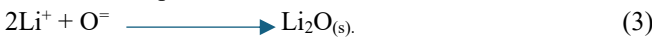
The hybrid fuel cell sketched in Figure 1 is intended to be operated over the temperature range 350–550 °C.

2(A). PRINCIPLES OF CELL OPERATION

At the cell cathode (C), oxygen reacts with electrons entering from the external electric circuit to form oxide ions, O^- ; based on the overall electrode kinetics; The oxide ions migrate through the scandia – doped zirconia (Electrolyte #1), to the magnesia immobilized eutectic mixture of lithium chloride and potassium chloride (Electrolyte #2). There the oxide ions react with the lithium ions to form di-lithium monoxide ($\text{Li}_2\text{O}(s)$) at any temperature over the intended cell operational temperature range of 350 – 550 °C. During the cell discharge period, at cell anode (A), lithium from lithium-aluminum alloy turns into lithium ions and electrons. Electrons enter the external electric load circuit; whereas the produced lithium ions migrate to the spatial region in the cell occupied by the Electrolyte #2. The overall cell reaction is as follows:



In the cell spatial region occupied by the eutectic mixture of lithium chloride and potassium chloride, the following reaction takes place:



Addition of Equation (1), (2) & (3) leads to:



$$\nu_{\text{LiAl}(s)} = -2, \nu_{\text{O}_2(g)} = -\frac{1}{2}, \nu_{\text{Al}(s)} = +2, \nu_{\text{Li}_2\text{O}(s)} = +1.$$

The number of g-moles of electrons involved per g-mole occurrence of reaction (4) is, $n = 2$ (g-moles). Following [1], the reversible cell electric potential at a temperature $T[\text{K}]$ is given by

$$E_T = E_T^0 - \left(\frac{RT}{nF}\right) \ln[\pi_i a_i^{\nu_i}], \quad (5)$$

where $a_i =$ activity of a species i involved in the overall cell reaction (4).

Note that the standard state cell electric potential at temperatures $T[\text{K}]$; E_T^0 is the electric cell potential where a_i of each species is equal to unity. Equation (5) for the cell reaction (4) becomes,

$$E_T = E_T^0 - \left(\frac{RT}{nF}\right) \ln \left[a_{\text{LiAl}(s)}^{\nu_{\text{LiAl}(s)}} a_{\text{O}_2(g)}^{\nu_{\text{O}_2(g)}} a_{\text{Al}(s)}^{\nu_{\text{Al}(s)}} a_{\text{Li}_2\text{O}(s)}^{\nu_{\text{Li}_2\text{O}(s)}} \right] \quad (6)$$

$$E_T = E_T^0 - \left(\frac{RT}{2F}\right) \ln \left[a_{\text{LiAl}(s)}^{-2} a_{\text{O}_2(g)}^{-\frac{1}{2}} a_{\text{Al}(s)}^2 a_{\text{Li}_2\text{O}(s)}^1 \right] \quad (7)$$

$$E_T = E_T^0 - \left(\frac{RT}{2F}\right) \ln \left[\frac{a_{\text{Al}(s)}^2 a_{\text{Li}_2\text{O}(s)}^1}{a_{\text{LiAl}(s)}^2 \sqrt{a_{\text{O}_2(g)}}} \right] [=] \text{ (volt)}. \quad (8)$$

Here, for solid aluminum, di-lithium monoxide and lithium-aluminum alloy; $a_{\text{Al}(s)} = a_{\text{Li}_2\text{O}(s)} = a_{\text{LiAl}(s)} = 1$; i.e., the activity of each of these solid-phase species is equal to unity. Consequently, Equation (8) reduces to:

$$E_T = E_T^0 - \left(\frac{RT}{2F}\right) \ln \left[\frac{1}{\sqrt{a_{\text{O}_2(g)}}} \right] [=] \text{ (volt)}. \quad (9)$$

$$\text{Or, } E_T = E_T^0 - \left(\frac{RT}{2F}\right) \ln \left[a_{\text{O}_2(g)}^{-\frac{1}{2}} \right] [=] \text{ (volt)}. \quad (10)$$

The activity of oxygen_(g) is given as:

$$a_{\text{O}_2(g)} = \frac{\hat{\phi}_{\text{O}_2(g)}^{\nu_{\text{O}_2(g)}} P^{\nu_{\text{O}_2(g)}}}{P^0} = \frac{\hat{\phi}_{\text{O}_2(g)}^{\nu_{\text{O}_2(g)}} y_{\text{O}_2(g)}^{\nu_{\text{O}_2(g)}} P^{\nu_{\text{O}_2(g)}}}{P^0} \quad (11)$$

where $\hat{\phi}_{\text{O}_2(g)} (= \hat{\phi}_{\text{O}_2(g)}(T, y_j(g), P)) =$ fugacity coefficient of oxygen species), to account for its non-ideal behavior in the gas phase when the gas pressure, P , is high and the interaction between the molecules are strong so that the assumption of ideal-gas mixture is really not a valid one. $y_{\text{O}_2(g)} =$ oxygen mole fraction in the dry oxidant feed, e.g., in dry air feed, $y_{\text{O}_2(g)} = 0.21$; $P =$ pressure of the oxidant feed mixture, e.g., dry air, in the oxidant flow chamber [bar]; $P^0 =$ the standard state pressure = 1[bar].

Combining of equations (10) & (11) leads to;

$$E_T = E_T^0 - \left(\frac{RT}{2F}\right) \ln \left[\frac{1}{\left(\frac{\hat{\phi}_{\text{O}_2(g)}^{\nu_{\text{O}_2(g)}} y_{\text{O}_2(g)}^{\nu_{\text{O}_2(g)}} P^{\nu_{\text{O}_2(g)}}}{P^0}\right)^{\frac{1}{2}}} \right] \quad (12)$$

For $P \leq 10$ bar; it is quite reasonable to assume $\hat{\phi}_{\text{O}_2(g)} \cong 1.0$.

The equation (12) reduces to

$$E_T = E_T^0 - \left(\frac{RT}{2F}\right) \ln \left[\frac{1}{\left(y_{\text{O}_2(g)}^{\frac{1}{2}}\right) \left(\frac{P}{P^0}\right)^{\frac{1}{2}}} \right] \quad (13)$$

For the case of pure-dry oxygen feed, $y_{O_2}(g) = 1$ in Equation (13) and then, from Equation (13), we obtain

$$E_T = E_T^0 - \left(\frac{RT}{2F}\right) \ln \left(\frac{1}{\left(\frac{P}{P^0}\right)^{\frac{1}{2}}} \right) \quad (14)$$

The standard-state cell electric potential, E_T^0 , is given by

$$E_T^0 = \left(\frac{-\Delta G_T^0}{nF}\right) = \left(\frac{-\Delta G_T^0}{2F}\right) \quad (15)$$

The standard-state Gibbs free energy change, ΔG_T^0 , at the cell temperature, T[K], is given [2] as

$$\Delta G_T^0 = \Delta G_{T_0}^0 \left(\frac{T}{T_0}\right) + \Delta H_{T_0}^0 \left(1 - \frac{T}{T_0}\right) + \frac{1}{T} \int_{T_0}^T \Delta C_P^0 dT - \int_{T_0}^T \left(\frac{\Delta C_P^0}{T}\right) dT \quad (16)$$

where $\Delta G_{T_0}^0$ and $\Delta H_{T_0}^0$ are, for the reaction, Equation (4), the Gibbs free energy and enthalpy changes at the reference temperature, $T_0 = 198.15 \text{ K}$; with the chemical species involved in the reaction being in their respective standard states.

The standard state $\Delta H_{T_0}^0$, $\Delta G_{T_0}^0$ and heat capacity ΔC_P^0 are given as

$$\Delta H_{T_0}^0 = \sum_i \nu_i H_{i,T_0}^0 = \sum_i (\nu_i \Delta H_{f_i,T_0}^0) = \left[(2H_{Al(s),T_0}^0 + H_{Li_2O(s),T_0}^0) - (2H_{LiAl(s),T_0}^0 + \frac{1}{2}H_{O_2(g),T_0}^0) \right] \quad (17)$$

$$\Delta H_{T_0}^0 = \left[(2\Delta H_{f,Al(s),T_0}^0 + \Delta H_{f,Li_2O(s),T_0}^0) - (2\Delta H_{f,LiAl(s),T_0}^0 + \frac{1}{2}\Delta H_{f,O_2(g),T_0}^0) \right] \quad (18)$$

Similarly,

$$\Delta G_{T_0}^0 = \left[(2\Delta G_{f,Al(s),T_0}^0 + \Delta G_{f,Li_2O(s),T_0}^0) - (2\Delta G_{f,LiAl(s),T_0}^0 + \frac{1}{2}\Delta G_{f,O_2(g),T_0}^0) \right] \quad (19)$$

By convention for pure elemental species in their standard states at $T_0 = 198.15 \text{ K}$, $\Delta H_{f,i(element),T_0}^0 = \Delta G_{f,i(element),T_0}^0 = 0.0 \text{ [J} \cdot \text{mol}^{-1}]$. Then, equations (18) and (19) are reduced to

$$\Delta H_{T_0}^0 = \Delta H_{f,Li_2O(s),T_0}^0 - 2\Delta H_{f,LiAl(s),T_0}^0, \text{ [J} \cdot \text{mol}^{-1}] \quad (20)$$

$$\Delta G_{T_0}^0 = \Delta G_{f,Li_2O(s),T_0}^0 - 2\Delta G_{f,LiAl(s),T_0}^0, \text{ [J} \cdot \text{mol}^{-1}] \quad (21)$$

Also, ΔC_P^0 of the reaction, equation (4), is given by

$$\Delta C_P^0 = \sum_i (\nu_i \cdot C_{P,i}^0) = \left[(2C_{P,Al(s)}^0 + C_{P,Li_2O(s)}^0) - (2C_{P,LiAl(s)}^0 + \frac{1}{2}C_{P,O_2(g)}^0) \right] \quad (22)$$

where $C_{P,i}^0$ = (heat-capacity of a species i in its defined standard-state at temperature T[K]) = $C_{P,i}^0(T) \text{ [J} \cdot \text{mol}^{-1} \cdot \text{K}^{-1}]$

Using equations (16), (20), (21) and (22), one computes ΔG_T^0 and hence, E_T^0 from Equation (15). Then one can calculate E_T , from Equation (14) at any cell temperature, $T[\text{K}]$.

2(B) ESSENTIAL PROPERTIES OF THE CELL COMPONENTS

Cell cathode (C): Porous strontia-doped lanthanum manganite (solid), $\text{La}_{1-x}\text{Sr}_x\text{MnO}_3$ ($0.10 < x < 0.18$). Presence of strontium bestows p-type electronic conductivity [3]. The oxygen mass transfer to the electrochemical reaction active

sites throughout the cathode is facilitated by the porosity in it. In the solid composite of $[(\text{La}_{1-x}\text{Sr}_x\text{MnO}_3) - \text{LSM}]$ and yttria-stabilized zirconia $[(\text{ZrO}_2)_{1-y}(\text{Y}_2\text{O}_3)_y] - \text{YSZ}$ oxygen vacancy defects facilitate the O^{2-} anion mass transport.

Molecular oxygen from the cell cathode-side chamber diffuses through pores in the cathode for its contact with the reaction active sites. The LSM particles receive electrons from the cathode-current collector during the cell discharge period. Molecular oxygen is assumed to be chemisorbed on the LSM-particle surface. The chemisorbed molecular oxygen decomposes into the oxygen atoms while receiving electrons. Thus, singly charged O^- ions are generated on the surfaces of LSM particles. These anions migrate on the LSM-particle surface to the three-phase boundary where O^- ions are transferred to the YSZ-particle surface in the form of O^{2-} anions with the creation of electron holes in the bulk of the LSM particles. The doubly charged O^{2-} anions migrate on the YSZ particle surfaces to the interface between the cathode and electrolyte #1.

In accordance with [4], the oxide anion transport through the bulk of LSM particles is assumed negligible. Furthermore, O^{2-} anions transport through the bulk of the YSZ particles is also assumed negligible. Using the information provided in [5], the developed expression to calculate the electrical conductivity in the cathode is given below.

$$\sigma^c = 1000.045 e^{-\frac{4605.2}{T}} \left[\frac{\text{S}}{\text{cm}} \right] \quad (23)$$

Where temperature, T is in degree K.

Electrolyte 1 (Electro #1): Solid solution of scandia in zirconia, $[(\text{ZrO}_2)_{1-x}(\text{Sc}_2\text{O}_3)_x]$: The primary requirements [4] for an electrolyte to function effectively are: The oxide anion O^{2-} ionic conductivity must be high (e.g., of the order of $0.1 \frac{\text{S}}{\text{cm}}$ at an operating temperature of the cell), low electronic conductivity, thermodynamic and chemical stability over a wide temperature range (e.g., room temperature to 1000°C) and reliable mechanical properties [6]. The cubic fluorite type phase [7] of the scandia-stabilized zirconia has the highest ionic conductivity among all zirconia solid solutions [8]. It is because the ionic radius of the cation, Sc^{3+} , 0.087nm is the closest to the ionic radius of the cation, Zr^{4+} , 0.084nm . This results in lower internal stress and steric-hindrance effect for the migration of the oxide anions, O^{2-} [9]. At about $500\text{-}600^\circ\text{C}$, the high conductivity cubic phase transformed to the rhombohedral phase. Consequently, this results in ionic conductivity degradation at cell operational temperatures. One way to suppress this degradation is to introduce the second dopant (co-dopant) to the electrolyte 1 structure; for example, yttria oxide, $\text{Y}_2\text{O}_3(\text{s})$.

Electrolyte 2 (Electro #2): It is the eutectic mixture of (lithium chloride, LiCl , and potassium chloride, KCl) with the magnesium oxide, $\text{MgO}(\text{s})$, the ceramic solid particles as the immobile agents for the fused (melt) eutectic mixture of the lithium and potassium chloride salts; the melting point of magnesium oxide is 2852°C , whereas the melting point of

LiCl_(s) and KCl_(s) is approximately 610 and 771 °C, respectively. The density of the mixture of magnesium oxide (35% by weight) and (the eutectic mixture of lithium chloride and potassium chloride (58.8 and 41.2 mole %)) is $1.65 \frac{gm}{cm^3}$ and the electric conductivity of this ternary component mixture [10] is $0.7647 \frac{S}{cm}$.

Molecular weights (in fact, molecular masses) of LiCl, KCl, and MgO are 42.397, 74.555, and $40.311 \frac{gm}{mole}$, respectively. Based on the above-mentioned information, the volume fraction occupied by the (LiCl-KCl) eutectic mixture in the cell Electrolyte 2 (Electro #2) is $\epsilon_{eutectic} = 0.8046$. The effective area for the Li⁺, K⁺, and Cl⁻ ion transport in the Electrolyte 2 is given as

$$a_{effective} (= \epsilon_{eutectic}) = \left(\frac{0.8046 \text{ cm}^2 \text{ for the ion transport}}{\text{cm}^2 \text{ of the total area of the Electro 2 perpendicular to the } X^A\text{-coordinate}} \right) \quad (24)$$

The eutectic current density, $i_{eutectic}$, through the cell electrolyte 2 is now given as:

$$i_{eutectic} = \frac{i_{geom}}{a_{effective}} \left(\frac{\text{amp}}{\text{cm}^2 \text{ of the eutectic mixture occupied spatial area}} \right) \quad (25)$$

where i_{geom} = magnitude of the geometric current density through the cell electrolyte 2, $\left(\frac{\text{amp}}{\text{cm}^2} \right)$. During the cell discharge period for the delivery of electric power to an external electric load, the ohmic voltage drop (loss) in the cell electrolyte 2 is given by

$$[(\Delta\Phi)_{\Omega-loss}^{Electro \#2}] = \left(\frac{l^{Electro \#2}}{a_{effective} \kappa_{eutectic}} \right) i_{geom}, \text{ (volt)} \quad (26)$$

where the ionic conductivity of the LiCl-KCl eutectic mixture as a function of temperature is given [11,12] by

$$\kappa_{eutectic} = a + bT + cT^2, \left(\frac{S}{cm} \right) \quad (27)$$

Where $a = -5.6492 \left(\frac{S}{cm} \right), b = 1.3732 \times 10^{-2} \left(\frac{S}{cm-K} \right)$ and $c = -5.1788 \times 10^{-6} \left(\frac{S}{cm-K^2} \right)$. A reader interested in gaining more insight into the behavior of the LiCl-KCl eutectic is referred to [13].

Cell anode (A): Lithium-aluminum alloy (Li_xAl) in contact with the electrolyte 2 (Electro #2), where x = number of g-atoms of lithium per g-atom of aluminum metal in the alloy. It is well known that the charge carriers in the metallic conductors are ‘free electrons’. The electrical conductivity (in fact electronic conductivity) in a metal is usually represented as,

$$\sigma_e = n_e q_e \mu_e, \left(\frac{S}{cm} \right) \quad (28)$$

where n_e = number concentration of free (mobile) electrons per unit volume of a metallic conductor, q_e = magnitude of change on an electron, and μ_e = mobility of the mobile electrons in a metallic conductor such as aluminum; it is the charge carrier drift velocity divided by an electric field strength, (cm². volt⁻¹. sec⁻¹).

When both positive (e.g., lithium ions in the lithium melt state) and negative (e.g., electrons in the solid aluminum state) charge carriers contribute to the charge conduction, the electric conductivity is given as

$$\sigma = n_p q_p \mu_p + n_n q_n \mu_n, \left[\frac{S}{cm} \right] \quad (29)$$

Positive and negative charge carriers are denoted by the subscripts p and n, respectively. The magnitude of q per electron, electron hole, or monovalent ion is (0.16 x 10⁻¹⁸C). For a multivalent ion, M^{Z+} and X^{Z-}, $q_{Z+} = Z_+ (0.16 \times 10^{-18}C)$ or $|q_{Z-}| = |Z_-| \times (0.16 \times 10^{-18}C)$.

In the cell operational temperature range of 350-550 °C, aluminum in the lithium-aluminum alloy is most likely to remain in the solid state, whereas lithium would be in the liquid state. Resistivity of the annealed aluminum at the room temperature (rt) of 20 °C ($\equiv 293.15 K$) [14] is,

$$\rho_{Al(s),rt} = 28.28 \times 10^{-7}, \text{ (ohm}\cdot\text{cm)} \quad (30)$$

The aluminum electric resistivity at a temperature, T[K], is given by

$$\rho_{Al(s)} = \rho_{Al(s),rt} [1 + \alpha_{Al(s)} (T - T_{rt})] = \rho_{Al(s),rt} [1 + \alpha_{Al(s)} (T - 293.15)], \text{ (ohm}\cdot\text{cm)} \quad (31)$$

where, $\alpha_{Al(s)} = 0.0039 [K^{-1}]$.

The electric resistivity of the lithium melt [15] is given by the following correlating polynomial

$$\rho_{Li(liq)} = (2.256 + 0.06665T - 4.255 \times 10^{-5}T^2 + 1.398 \times 10^{-8}T^3) \times 10^{-6}, \text{ (ohm}\cdot\text{cm)} \quad (32)$$

where, T = liquid phase lithium temperature [K].

Over the above-mentioned temperature range of our current interest, the aluminum atoms in the Li_xAl alloy would be in the solid aluminum state. The mass transport process in Li_xAl alloy would be dominated by the movement of lithium atoms or ions. This assumption is supported by the NMR studies on lithium-aluminum alloy [16].

The electric conductivities of solid aluminum and liquid lithium are, respectively, given as

$$\sigma_{Al(s)} = \frac{1}{\rho_{Al(s)}}, \left[\frac{S}{cm} \right] \quad (33)$$

$$\sigma_{Li(liq)} = \frac{1}{\rho_{Li(liq)}}, \left[\frac{S}{cm} \right] \quad (34)$$

The electric conductivity of Lithium-aluminum alloy, Li_xAl, is given as:

$$\sigma_{alloy} = \left(\frac{\sigma_{Al(s)} + X\sigma_{Li(liq)}}{1+X} \right), \left[\frac{S}{cm} \right] \quad (35)$$

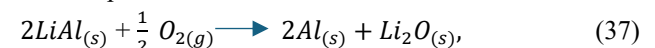
The ohmic voltage loss in the Li_xAl alloy anode at an all-geometric current density, i_{geom} , is given by

$$[(\Delta\Phi)_{\Omega-loss}^A] = \left[\left(\frac{l^A}{\sigma_{alloy}} \right) i_{geom} \right], \text{ (volt)} \quad (36)$$

where l^A = thickness of the cell anode.

During the cell discharge period, the lithium content of the cell alloy anode would decrease. Consequently, the electric conductivity, σ_{alloy} , is likely to change as expressed by Equation (35).

In correspondence with the overall cell reaction:



the amount of lithium consumed, corresponding to the cell geometric current density, i_{geom} , is the time period of t (seconds) during the cell discharge is given by

$$[-(\Delta N_{Li})]_{geom} = \left(\frac{\int_0^t i_{geom} dt}{F} \right), \left(\frac{g\text{-atoms of lithium consumed}}{cm^2_{geom}} \right). \quad (38)$$

The lithium amount in the cell anode, during the cell discharge period, at time, t (sec), is given as

$$(N_{Li})_{geom} = \left[(N_{Li,initial})_{geom} + (\Delta N_{Li})_{geom} \right] = \left[(N_{Li,initial})_{geom} - \left(\frac{\int_0^t i_{geom} dt}{F} \right) \right], (g\text{-atoms of lithium}). \quad (39)$$

It is here again noted that the amount of aluminum in the anode, over the temperature range of 350-550 °C, would remain invariant during the period of the cell discharge, i.e., the g -atoms of $Al_{(s)}$ at time, t (sec), during the discharge period, $N_{Al(s),geom} = N_{Al(s),initial}$. So, the ratio of the g -atoms of lithium to the g -atoms of aluminum, during the cell discharge period, at time t (sec) is given as

$$X = \left(\frac{(N_{Li})_{geom}}{(N_{Al(s),initial})_{geom}} \right) = \left[\frac{(N_{Li,initial})_{geom}}{(N_{Al(s),initial})_{geom}} - \frac{\int_0^t i_{geom} dt}{F(N_{Al(s),initial})_{geom}} \right] \quad (40)$$

Or

$$X = \left[X_0 - \frac{\int_0^t i_{geom} dt}{F(N_{Al(s),initial})_{geom}} \right] \quad (41)$$

where X_0 = ratio of the g -atoms of lithium to the g -atoms of aluminum at the initial state of the cell anode at time, $t = 0.0$ sec.

At a constant current cell discharge, Equation (41) reduces to

$$X = \left[X_0 - \frac{i_{geom} t}{F(N_{Al(s),initial})_{geom}} \right] \quad (42)$$

During the cell discharge period, the parameter X in equation (42) is likely to decrease. At some time, $t = t_{exhaust}$ (sec); X would become zero, i.e., the entire lithium amount in the cell anode would have been completely consumed.

The ohmic voltage loss in the cell anode, during the cell discharge period, would change as indicated by equations (35) and (36).

Figure 2 of Ref.[16] provides the information about the lithium-aluminum alloy phases as a function of x in Li_xAl at 423 °C. The solid solubility of lithium in aluminum is 9.2 atomic percent (α -phase). The β -phase exists for the lithium solubility in aluminum for the lithium atomic percent from 46.8 to 56%. The γ -phase prevails between 60.3 and 61.7 atomic percent of lithium. The two-phase ($\alpha + \beta$), region exists between the α - and β - phases and the ($\beta + \gamma$) phase region exists between the β - and γ - phases. The study of the works by the various authors reported in [15] leads us to state that the Li_xAl alloy in the cell anode would undergo phase transformations during the discharge period of the hybrid fuel cell: Li_xAl / (oxygen or dry air).

3. TYPICAL EXAMPLE CALCULATED DATA at T = 678.15K (= 405°C):

(a) For $\left(\frac{P}{P_0}\right) = 1$ and y_{O_2} (in air) = 0.21; the cell e.m.f. or open-circuit voltage from equation(14), $E_T = 2.3241$ volt.

(b) The ohmic voltage loss in the various components of the cell at $i_{geom} = 0.10 \text{ amp} \cdot \text{cm}^{-2}_{geom}$:

(b-1) Cell Cathode (C):

For $l^C = 20\mu\text{m}$, $x = 0.2$ in $(La_{1-x}Sr_xMnO_3)$ (s) using equation (23) and

$$[(\Delta\Phi)_{\Omega-loss}^C] = \left(\frac{l^C \cdot i_{geom}}{\sigma^C} \right), (\text{volt}) = 1.7792 \times 10^{-4} (\text{volt}).$$

(b-2) Electrolyte 1 (Electro #1):

Thickness of the electrolyte 1, $l^{Electro \#1} = 10\mu\text{m}$

$$[(\Delta\Phi)_{\Omega-loss}^{Electro \#1}] = \left(\frac{l^{Electro \#1} \cdot i_{geom}}{\kappa^{Electro \#1}} \right) \cong 1.3620 (\text{volt})$$

(b-3) Electrolyte 2 (Electro #2):

Thickness of the electrolyte 2, $l^{Electro \#2} = 500\mu\text{m}$

$$[(\Delta\Phi)_{\Omega-loss}^{Electro \#2}] = \left(\frac{l^{Electro \#2} \cdot i_{geom}}{\alpha_{effective} \cdot \kappa_{eutectic}} \right) = 4.8 \times 10^{-3} (\text{volt})$$

(b-4) Cell Anode (A):

Thickness of the cell anode, $l^A = 25\mu\text{m}$

$$[(\Delta\Phi)_{\Omega-loss}^A] = \left(\frac{l^A \cdot i_{geom}}{\sigma_{LiAl \text{ alloy}}} \right) = 1.7685 \times 10^{-9} (\text{volt})$$

Note: The above given calculated data are based on the assumption that the voltage losses due to the contact resistances between the cell components are negligible. Also, in the absence of electro-kinetics rate law equations (based on experimental data); the electro-kinetics polarization voltage losses in the cell cathode and anode electrodes are assumed negligible.

(b-5) The sum of the above given voltage losses at T = 678.15 K and $i_{geom} = 0.10 \text{ amp} \cdot \text{cm}^{-2}$ is:

$$[(\Delta\Phi)_{\Omega-loss}^{Total}] = 1.3670 (\text{volt}).$$

(C) Based on the above given calculated data, the predicted cell voltage of the cell operation at 678.15K and $i_{geom} = 0.10 \text{ amp} \cdot \text{cm}^{-2}$ during the cell discharge period is

$$E = \left[E_T - [(\Delta\Phi)_{\Omega-loss}^{Total}] \right] = [2.3241 - 1.3670](\text{volt}) = 0.9571(\text{volt}).$$

4. CONCLUSIONS DRAWN FROM THE CALCULATED DATA IN SECTION 3:

For the cell of the type, sketched in Figure 1 operated at 678.15 K and $i_{geom} = 0.10 \text{ amp} \cdot \text{cm}_{geom}^{-2}$ during its discharge period, the calculated data presented in Section 3 leads us to the following:

- (a) The ohmic voltage loss in the cell anode is negligible; whereas that in electrolyte 1, electrolyte 2, and cathode, respectively, are: 1.3620, 0.0048, and 0.0002 *volt*.

It is obvious that the ohmic voltage loss in electrolyte 1 of thickness, $10 \mu\text{m}$, is the dominant cell voltage loss (i.e., 1.3620 (*volt*)). To reduce the cell ohmic voltage loss, it is suggested that the thickness of the electrolyte 1 membrane be less than $10 \mu\text{m}$ during the build-up of an experimental physical system: for example, $l^{Electro \#1} = 5 \mu\text{m}$.

- (b) The predicted open-circuit cell voltage is 2.3241 *volt*.
- (c) The predicted available cell voltage for the delivery of electric power to an external-circuit electric load is about 0.9571 *volt* at $i_{geom} = 0.10 \text{ amp} \cdot \text{cm}_{geom}^{-2}$.

Finally, it is suggested that the experimental electrode-kinetics data; especially, for the porous cathode (C), of the cell shown in Figure 1 be acquired for the development of the intrinsic electrochemical reaction-rate law of the Butler-Volmer type [17].

REFERENCES

1. G. Prantice, Electrochemical Engineering Principles, p.37, Prantice-Hall, Inc. (1991).
2. J.M. Smith, H.C. Van Ness, and M.M.Abbott, Introduction to Chemical Engineering Thermodynamics, p.494; 2005, 7th edition; McGraw-Hill Higher Education, Inc.
3. A.J. Appleby and F.R. Foulkes, Fuel Cell Handbook, pp.390-410, (1989). Van Nostrand Reinhold, New York.
4. A. Banerjee and O. Deutschmann, Elementary kinetics of the oxygen reduction reaction on LSM-YSZ composite cathodes. Journal of Catalysis, Vol. 346, February 2017, pp. 30-49.
5. R.J. Wlglusz, et al. Conductivity and electric properties of $\text{La}_{1-x}\text{Sr}_x\text{MnO}_3$ nanopowders. Journal of Rare Earths 27(4), pp. 651-654 (August 2009). DOI: 10.1016/S1002-0721(08)60308-7
6. M.A. Borik, et al. Structure and Conductivity of yttria- and scandia-doped zirconia crystals by skull melting. J Am Ceram Soc. 2017; 100 : 5536-5547. (<https://doi.org/10.1111/jace.15074>)
7. F.A. Cotton and G. Wilkinson, Advanced Inorganic Chemistry, p.51; 1972, 3rd edition. John Wiley & Sons, Inc. New York.
8. Y. Arachi, et al. Electrical Conductivity of the $\text{ZrO}_2\text{-Ln}_2\text{O}_3$ (Ln-Lanthnides) system. Solid state Ionics. 1991; 121: 122-139.
9. R.J. Stafford, S.J. Rothman and J.L. Routbort. Effect of dopant size on the ionic conductivity of cubic stabilized ZrO_2 . Solid state Ionics. 1989; 37: 67-72.
10. S. Rattanaphan and P. Kamlahasuth. Enhanced electric conductivity by modifying LiCl-KCl mole fraction at high temperature. Proceedings of 76th, the IIER International Conference, Tokyo, Japan, 20th July 2016; ISBN: 978-93-86083-61-6.
11. G.J. Jans, et al. J. Rhys. Chem. Ref. Data, Vol. 4, p.871 (1975).
12. J-Y. Kim, et al. Electrical conductivity measurement of molten salts using two-electrode alternative current impedance method. Asian Journal of Chemistry; Vol. 25, No (12) (2013), pp. 7028-7030. (<http://dx.doi.org/10.14233/ajchem.2013.10>)
13. D. Bernardi, et al. Mathematical Modeling of LiAl/LiCl, KCl/FeS cells. J. of the Electrochemical Society (ECS), Vol. 135, No. 12, pp. 2922-2931 (December 1988).
14. J.F. Shackelford, Introduction to Materials Science for Engineers, Chapter 11, pp. 528-544. (1992, 3rd edition), Macmillan Publishing Company, New York.
15. H.W. Davison, Compilation of Thermophysical Properties of Liquid Lithium. NASA Technical Note; NASA TN D-4650. National Aeronautics and Space Administration. Washington, D.C. July 1968.
16. C.J. Wen, et al. Thermodynamic and Mass Transport Properties of “LiAl”. J. Electrochem. Soc.: Solid-State Science and Technology; Vol. 126, No.12 (December 1979).
17. J. Newman and N.P. Balsara. Electrochemical Systems, p. 174. (2021, 4th edition) John Wiley & Sons Inc.